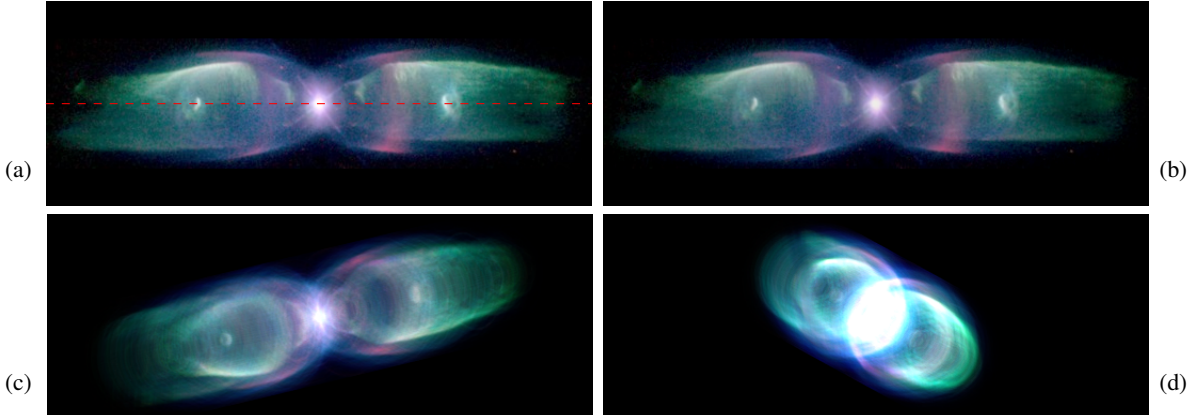


# Fast Image-Based Modeling of Astronomical Nebulae

Stephan Wenger<sup>1</sup>, Dirk Lorenz<sup>2</sup>, and Marcus Magnor<sup>1</sup>

<sup>1</sup>Institut für Computergraphik, TU Braunschweig, Germany

<sup>2</sup>Institut für Analysis und Algebra, TU Braunschweig, Germany



**Figure 1:** The Butterfly Nebula M2-9, located more than 2 000 light-years from Earth, is a typical bipolar planetary nebula, shaped by two polar jets originating from the central binary star. From a single input image (a), our algorithm produces a volumetric model based on symmetry assumptions without any further user interaction. The model faithfully reproduces the input image when rendered from the original viewpoint (b) and can interactively be rendered from arbitrary novel views (c)–(d). The  $122 \times 512 \times 122$  voxel model was reconstructed in 14.7 seconds on a 4-core Intel® Core™ i7-960 CPU. Original image credits: Bruce Balick (University of Washington), Vincent Icke (Leiden University), Garrett Mellemma (Stockholm University), and NASA.

## Abstract

Astronomical nebulae are among the most complex and visually appealing phenomena known outside the bounds of the Solar System. However, our fixed vantage point on Earth limits us to a single known view of these objects, and their intricate volumetric structure cannot be recovered directly. Recent approaches to reconstructing a volumetric 3D model use the approximate symmetry inherent to many nebulae, but require several hours of computation time on large multi-GPU clusters. We present a novel reconstruction algorithm based on group sparsity that reaches or even exceeds the quality of prior results while taking only a fraction of the time on a conventional desktop PC, thereby enabling end users in planetariums or educational facilities to produce high-quality content without expensive hardware or manual modeling. In principle, our approach can be generalized to other transparent phenomena with arbitrary types of user-specified symmetries.

Categories and Subject Descriptors (according to ACM CCS): I.3.8 [Computer Graphics]: Applications—J.2 [Computer Applications]: Physical Sciences and Engineering—Astronomy

## 1 Introduction

Astronomical nebulae are a major subject of interest in astronomy and astrophysics. Since the advent of telescopes,

they have been studied and catalogued. Modern research has shed light on their important role in the evolution of the universe: some types of nebulae provide the matter from which

stars and planetary systems are formed; others, **expelled by stars at the end of their lifetime**, disperse the heavy elements generated by stellar nucleosynthesis.

Many representatives of the latter class are so-called *planetary nebulae*, named such because the first observers mistook them for planets due to the **limited resolution of their telescopes**. More recent observations (e.g., by the Hubble Space Telescope), however, reveal their often complex and intricate structure. Planetary nebulae form when stars of a certain size have used up the hydrogen fuel in their cores and become red giants, inflating to many times their original size. The outer layers of the star are swept away by stellar winds and form an expanding nebula. The atoms in the nebula become ionized by ultraviolet radiation from the remaining star, begin glowing at characteristic wavelengths, and can thus be observed using optical telescopes. The structure of the resulting nebula depends on the presence of many factors, including a possible companion star, a strong **magnetic field**, the surrounding **interstellar medium**, or internal hydrodynamic effects. Some of these factors favor the formation of rotationally symmetric structures, so that many planetary nebulae exhibit at least an approximate axial symmetry [Kwo07, KS05].

On the one hand, the mechanisms underlying planetary nebula formation and evolution are an active field of research in astronomy and astrophysics. On the other hand, their complex and beautiful structure, their important role for the chemical composition of the galaxy, and the fact that our Sun faces a similar fate all have contributed to the fact that planetary nebulae are a popular subject of educational shows in planetariums or dome theaters as well as astronomical visualization software. Yet, due to the large distance, only a single projection of a nebula is ever visible from Earth. This precludes us from directly deducing three-dimensional, volumetric models for visualization or scientific analysis. The realistic modeling of an astronomical nebula is therefore usually a manual process requiring skill and astronomical expertise, and can take a professional astronomer weeks or months even using specialized modeling software [SKW\*11, NGN\*01].

The difficulty of creating realistic, high quality volumetric models has led to a number of attempts to generate such models algorithmically from single images. Most notably, recent advances in automatic reconstruction [WAG\*12] have resulted in seven high-resolution models that have quickly been embraced by several vendors of planetarium software for use in their commercial digital full-dome visualization systems. However, the method requires long computation time on a large multi-GPU cluster, so that no further models have since been published.

With the proposed algorithm, we provide a method which for the first time enables planetarium show designers, presenters and educators to create their own high-quality volumetric content on commodity hardware that is already

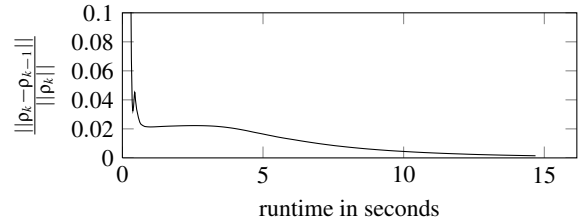


**Figure 2:** Convergence behavior for the reconstruction of M2-9 (Figure 1). The relative distance between subsequent iterates is plotted against the accumulated runtime.

present or affordable for end users. Our method usually requires no user input aside from a single image obtained from a public database on the internet and an approximate axis of symmetry. We exploit the approximate axial symmetry present in many nebulae to resolve the depth ambiguity using an optimization framework inspired by compressed sensing. An  $\ell_\infty$  group sparsity regularizer is used to promote symmetry and suppress image noise while an  $\ell_2$  data term enforces consistency with the observational data. Our method supports arbitrary types of user-defined symmetries and can thus in principle be used for other volumetric phenomena with different symmetry constraints. The resulting models can be displayed interactively using a simple GPU-based volume raycaster.

## 2 Related Work

Reconstructions of astronomical nebulae from the incomplete data available have been pursued by researchers from both astronomy and computer graphics, albeit with different goals: researchers in astronomy are interested in models that support or falsify their theories about nebula evolution while in the graphics community, high visual quality and realism are most important. In both cases, however, the lack of information allows any reconstruction to be at best plausible and consistent with the data, but some ambiguity remains. For example, recent research suggests that some nebulae that were so far believed to have different shapes might actually share a common morphology [GDL\*11]. In astronomy, this ambiguity is usually resolved by making complex assumptions about the object's structure based on expert knowledge and, where available, additional data. For example, spectra with high frequency resolution can provide information about the velocities of gas particles by observing the Doppler shift of spectral lines. Often, a qualitative model is created by an astronomer, and the model parameters are subsequently fitted to the observational data [MSGH04, SM06, MFG11]. Alternatively, by linking the velocity to a three-dimensional position through a model of nebula evolution, an approximation to the three-dimensional shape can be obtained directly [MdFPL04, STR\*06]. Due to the difficulty of obtaining spatially resolved spectra, however, the resulting models

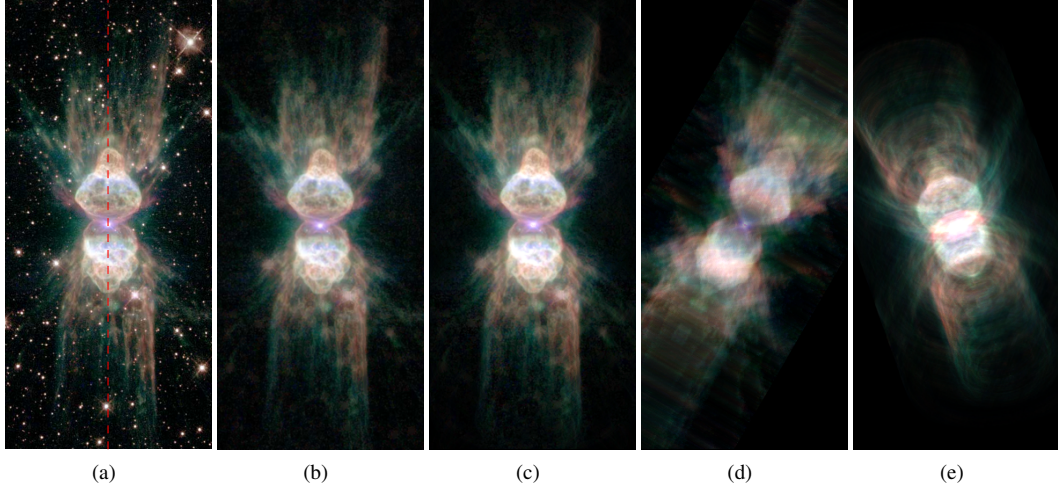


**Figure 3:** Mz 3, the so-called “Ant Nebula” (a), is a planetary nebula with a complex composite morphology. After removing the surrounding stars by manual editing (b), our algorithm reconstructed the  $235 \times 561 \times 460$  voxel model (c) in about 130 seconds. (d) and (e) show a view orthogonal to the symmetry axis and a random novel view, respectively. Original image credits: NASA, ESA, and The Hubble Heritage Team (STScI/AURA).

have low resolution, and the formulation of an appropriate model requires extensive expert knowledge.

Reconstruction based on symmetry assumptions has likewise originated in astrophysics [Lea91], but has since been adopted by computer graphics researchers as well. Early attempts created purely symmetric models without any asymmetric features [MKHD04, MKHD05], resulting in a lack of realism and perceived depth. Methods specifically targeting asymmetric nebulae, on the other hand, were not able to resolve the ambiguity in purely emissive objects like planetary nebulae [MHLH05]. The first method combining symmetry-based reconstruction with an ad-hoc method for the preservation of asymmetries was still prone to artifacts and did not scale well to higher resolutions [WAFMM09].

A recent optimization approach [WAG<sup>\*</sup>12] views the symmetric reconstruction as a special kind of tomographic reconstruction problem. The volume is tomographically reconstructed from several copies of the observed image rotated about the axis of symmetry, with the constraint that the view from the front exactly matches the observed image. This method effectively penalizes the deviation of a voxel from symmetry with the  $\ell_2$ -norm of the deviation. This favors solutions where many voxels deviate from asymmetry by a small amount, leading to streaking artifacts as well as rather flat intensity distributions that convey only a limited impression of depth. In our method, in contrast, the penalization effect is that of an  $\ell_1$ -norm, producing more localized and pronounced asymmetric features and a more intense impression of depth.

The computational bottleneck of the tomographic reconstruction problem in [WAG<sup>\*</sup>12] is the computation of many arbitrary three-dimensional projections, which are per-

formed in parallel on a large compute cluster with 32 CPUs and 64 GPUs. The communication overhead in the cluster as well as the limited GPU memory prevent scaling to resolutions much beyond  $512^3$  voxels. In contrast, our method computes only a single projection, greatly reducing the required amount of memory and computation time. Since this obviates the need for a distributed implementation, our method does not incur the associated communication overhead and scales well with increasing resolution. In addition, the projection is axis-aligned, leading to a more favorable memory access pattern, especially in a parallelized implementation. As a result, the proposed method works efficiently on a single multi-core commodity PC.

### 3 Imaging Model

We begin with a brief review of the physical process of image formation in a planetary nebula. Since the eruption of a dying star sweeps away most of the surrounding interstellar medium, planetary nebulae are typically devoid of dust and other large molecules that might cause absorption or scattering. Their optical image is therefore dominated by the emission from recombining electrons and ions. Thus, the intensity  $s(x, y)$  arriving on a camera pixel  $(x, y)$  is proportional to the accumulated emission density  $\rho(x, y, z)$  from all voxels  $(x, y, z)$  in its line of sight. We align the voxel grid with the image coordinate system, so that

$$s(x, y) = \frac{1}{\sqrt{n_z}} \sum_z \rho(x, y, z) , \quad \text{or} \quad s = P\rho , \quad (1)$$

when written in terms of a linear projection operator  $P$ . The normalization factor  $1/\sqrt{n_z}$ , where  $n_z$  is the number of voxels along the  $z$  axis, influences the convergence of the optimization algorithm; it bears no physical significance.

The reconstruction problem consists in finding an optimal density distribution  $\rho$  given an image  $s$ . It is obvious that this problem is severely ill-posed: many different  $\rho$  yield the same  $s$ . In the following, we describe a method for finding a maximally symmetric volume  $\rho$  in accordance with the observed image  $s$ .

#### 4 Group Sparsity and Optimization Problem

We describe the symmetry properties of a voxelized volume by defining a number of disjoint sets or *groups*  $G_i$  of voxels so that in a symmetric volume, the voxels within each group have equal intensities. In the case of axial symmetry, these groups are concentric rings: the voxels are binned according to the distance of their center from the axis of symmetry and its position along the axis. However, any configuration of disjoint sets can be used; this makes it possible to model arbitrary symmetries such as spherical symmetries, discrete rotational symmetries, mirror symmetries, translational symmetries, or rotational symmetries along user-specified paths. We denote the set of all voxel intensities in a group  $G_i$  as  $\rho_{\{G_i\}} = \{\rho(x, y, z) : (x, y, z) \in G_i\}$ . Where appropriate,  $\rho_{\{G_i\}}$  is interchangeably treated as a vector.

We propose to find a *maximally symmetric* volume  $\rho$  subject to a given image  $s$  by solving a *group sparsity* or *joint sparsity* problem [FR08] of the form

$$\arg \min_{\rho} \frac{1}{2} \|P\rho - s\|_2^2 + \tau \sum_i |G_i| \max \rho_{\{G_i\}} \quad (2)$$

subject to  $\rho \geq 0$ . The data term  $\frac{1}{2} \|P\rho - s\|_2^2$  enforces compatibility of the volume with the observed image. In particular, it fixes the integral over  $\rho$  along each viewing ray. The regularizer  $\sum_i |G_i| \max \rho_{\{G_i\}} = \sum_i |G_i| \|\rho_{\{G_i\}}\|_\infty$ , a weighted  $\ell_{1,\infty}$ -norm, penalizes the largest intensity value in each group. This means that the intensity becomes concentrated on as few groups as possible while satisfying the data term constraints, and voxels within the same group tend to have similar intensities. Scaling by the number of elements in the group  $|G_i|$  is necessary to avoid biasing the solution towards larger groups, where otherwise more intensity could be deposited with only one voxel penalized. The regularization factor  $\tau$  gives intuitive control over the deviation from the observational data in favor of a more symmetric result. Finally, the constraint  $\rho \geq 0$  enforces the result to be physically plausible in the sense that no negative emission can occur. The result is a volume  $\rho$  that is, in a certain sense, *as symmetric as possible* while being compatible with the data.

#### 5 Algorithm and Implementation

For solving (2), we adapt the *fast iterative shrinkage-thresholding algorithm* [BT09] to our group sparsity problem. Starting from initial volumes  $\rho_0 = 0$  and  $\rho_0^* = 0$ , we alternately perform a gradient descent step

$$\bar{\rho}_k = \rho_{k-1}^*(x, y, z) - \frac{1}{n_z} \sum_i \rho_{k-1}^*(x, y, i) + \frac{1}{\sqrt{n_z}} s(x, y) \quad (3)$$

and a regularization step

$$\rho_k(x, y, z) = p(\bar{\rho}_k) \quad (4)$$

followed by an update step

$$\rho_k^*(x, y, z) = (1 - a_k) \rho_k(x, y, z) + a_k \rho_{k-1}(x, y, z), \quad (5)$$

where

$$a_k = \frac{1 - t_{k-1}}{t_k}, \quad t_k = \frac{1 + \sqrt{1 + 4t_{k-1}^2}}{2}, \text{ and } t_0 = 1. \quad (6)$$

In (4),  $p(\bar{\rho})$  is the so-called *proximal mapping of the  $\ell_{1,\infty}$ -norm*; it computes a solution to the optimization problem

$$\arg \min_{\rho} \frac{1}{2} \|\rho - \bar{\rho}\|_2^2 + \tau \sum_i |G_i| \max \rho_{\{G_i\}} \quad \text{s.t.} \quad \rho \geq 0. \quad (7)$$

Equation (7) is *group separable* [WNF09], meaning it can be minimized by solving

$$\arg \min_{\rho_{\{G_i\}}} \frac{1}{2} \|\rho_{\{G_i\}} - \bar{\rho}_{\{G_i\}}\|_2^2 + \tau |G_i| \max \rho_{\{G_i\}} \quad (8)$$

subject to  $\rho_{\{G_i\}} \geq 0$  separately for each group  $G_i$ . Graphically speaking, the minimum is the vector from the orthogonal projection of  $\bar{\rho}_{\{G_i\}}$  onto the  $\ell_1$   $\tau |G_i|$ -ball  $\{\hat{\rho}_{\{G_i\}} : \|\hat{\rho}_{\{G_i\}}\|_1 \leq \tau |G_i|\}$  to  $\bar{\rho}_{\{G_i\}}$  [WNF09]. We implement (8) by adapting a fast algorithm for projections onto the  $\ell_1$ -ball [DSSC08] to our application. For each  $i$ , the updated  $\rho_{\{G_i\}}$  is computed from  $\bar{\rho}_{\{G_i\}}$  as shown in Algorithm 1, where  $\sum X$  denotes the sum over all elements of  $X$ , and min and max are defined element-wise.

**Algorithm 1** Computation of  $\rho_{\{G_i\}}$  from  $\bar{\rho}_{\{G_i\}}$  as in (8).

---

```

r ← τ |G_i|
ρ_{\{G_i\}} ← max(ρ_{\{G_i\}}, 0)
if ∑ ρ_{\{G_i\}} ≤ r then
    return 0
end if
u ← ρ_{\{G_i\}}
n ← 0
while u is not empty do
    choose a random element u_l from u
    u_< ← {u_j ∈ u : u_j < u_l}
    u_≥ ← {u_j ∈ u : u_j ≥ u_l}
    if ∑ u_≥ - (n + |u_≥|) u_l < r then
        r ← r - ∑ u_≥
        n ← n + |u_≥|
        u ← u_<
    else
        u ← u_≥ \ {u_l}
    end if
end while
return min(ρ_{\{G_i\}}, -r/n)

```

---

The computation of  $\bar{\rho}$  in (3) as well as the update of  $\rho^*$  in (5) can be performed in parallel for all image pixels and all voxels, respectively. The computation of  $p$  in (8) can be

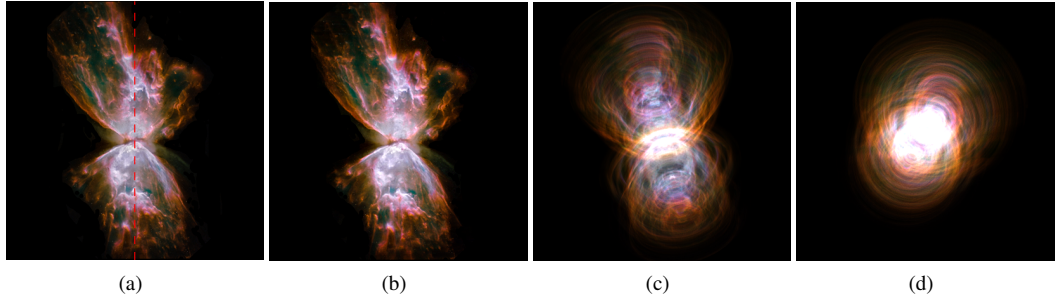


**Figure 4:** NGC 6302 is an unusually complex and dust-rich planetary nebula. From left to right: original image, reconstruction, novel views. Original image credits: Original image: NASA, ESA, and the Hubble SM4 ERO Team.

parallelized over all groups. The proposed algorithm therefore lends itself to a parallel implementation on a multi-core processor with shared memory. Parallelizing the code led to a speed-up by about a factor of 5.8 in our implementation.

Due to the relatively short computation time of the proposed method compared to previous approaches, intermediate results can constantly be monitored by the user in an interactive volume renderer, and the computation can be stopped as soon as satisfactory quality is reached, which is often after as few as 20 iterations. In an automated pipeline, the algorithm can be set to stop after a fixed number of iterations, or when the relative difference  $\|\rho_k - \rho_{k-1}\|/\|\rho_k\|$  between subsequent iterates falls below a specified threshold (cf. Figure 2).

## 6 Results

We evaluate our method on several planetary nebulae with approximate axial symmetry. False-color images of the nebulae were downloaded from several internet resources (e.g., [hubblesite.org](#)). The images were rotated to roughly align the symmetry axis with an image axis (dashed red lines) to create an optimal memory access pattern during reconstruction. Where necessary, stars were removed manually; this is indicated in the respective figures. To assign voxels to groups, the positions of their centers were transformed into cylindrical coordinates aligned with the axis of symmetry. The radial and axial coordinates were then divided by the radial and axial bin width, respectively, and rounded to the nearest integer. The tuple of rounded radial and axial coordinates uniquely determines the group for each voxel. In our experiments, we set both bin widths to the size of one voxel. To make the results comparable, we let the algorithm run for a full 100 iterations with  $\tau = 0.1$  in all cases. All experiments were performed on a 4-core Intel® Core™ i7-960 CPU.

Figure 1(a) shows the “Butterfly Nebula” M2–9, a typical bipolar nebula. We assumed that the axis of symmetry lies horizontally within the image plane and performed an automatic reconstruction with the default parameters. The resulting model, Figure 1(b), almost exactly reproduces the original image when rendered from the original viewpoint. Renderings from novel views, Figures 1(c) and (d), appear

smooth and plausible. Figure 2 shows the relative difference between subsequent iterates plotted over the accumulated runtime. After 100 iterations (about 14.7 s), it has dropped to a small fraction of its initial value, and no further change is visible in the reconstructed volume. For comparison, in prior work [WAG\*12], the reconstruction of M2–9 required two to eight hours (for 128 to 512 virtual projections, respectively) on a 64 GPU compute cluster at the same resolution.

For the “Ant Nebula” Mz 3, Figure 3(a), the inclinations of its several main axes with respect to the sky plane have been estimated at the range 10–30° [MW85]. Assuming an inclination of 30°, our algorithm produces a faithful model, Figure 3(c), in a little more than two minutes from an image with manually removed stars, Figure 3(b). The relatively long runtime is due in part to the less fortunate memory access pattern for inclined rings (for comparison, the runtime without inclination is about 51 seconds). Novel views of the model, Figures 3(d) and 3(e), show that in this case, the inclined projection contained enough information for a plausible reconstruction. However, for nebulae with larger inclination, the emission from different groups soon becomes too intermingled for a reconstruction from symmetry assumptions alone (cf. Figure 5).

Figure 7 shows additional reconstruction results: the Red Rectangle Nebula (HD 44179), a protoplanetary nebula; the Spirograph Nebula (IC 418), a planetary nebula; NGC 6826, a planetary nebula with a bright central star and two supersonic jets; the Saturn Nebula (NGC 7009), a popular planetary nebula; and the Calabash Nebula, a protoplanetary nebula with curiously dissimilar lobes. Table 1 gives an overview of the sizes of all reconstructed volumes and the respective runtimes. The angle shown represents the inclination of the symmetry axis with respect to the image plane. To investigate the behavior of our algorithm for very large input images, the Butterfly Nebula M2–9 was again reconstructed at the largest resolution available on [hubblesite.org](#) (664 × 2824 after rotation and cropping). The 3.5 GB volume could not be rendered using our GPU raycaster due to limited GPU memory; however, axis-aligned projections are included in the supplementary material.

Animations as well as comparisons to [WAG\*12] can be

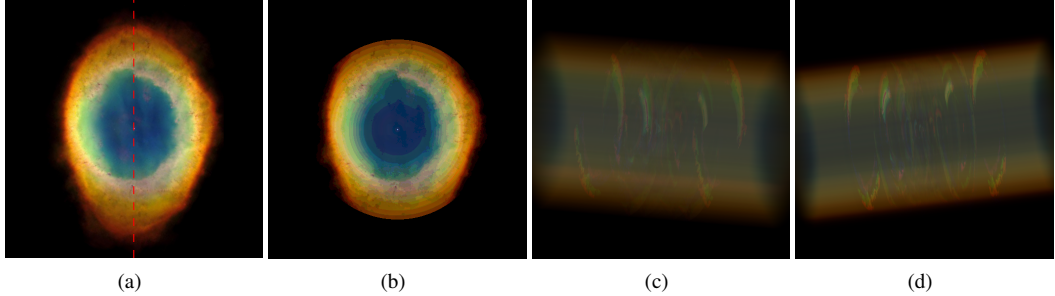


**Figure 5:** The axis of M57, the Ring Nebula, points almost directly towards Earth, making symmetry-based reconstruction impossible. From left to right: original image, failed reconstruction, novel views. Original image credits: The Hubble Heritage Team (AURA/STScI/NASA).

found in the supplementary video. The video also illustrates how in the prior work, rotations around the axis of symmetry often produced visible discontinuities, while our results typically show a much smoother transition.

## 7 Limitations and Future Work

Our algorithm attains its limits wherever any of its assumptions are violated. For example, the planetary nebula NGC 6302, Figure 4, contains unusual amounts of dust as well as many asymmetric finger-like structures in the outer lobes. While the original projection, Figure 4(b), faithfully reproduces the observed image, novel views, Figures 4(c) and (d), do not contain the structures one would have expected by looking at the image.

The symmetry axis of the Ring Nebula M57, Figure 5(a), almost exactly faces Earth. This makes it impossible to recover its three-dimensional structure from a single image using only symmetry assumptions. Consequently, the reconstructed volume is practically unusable, Figures 5(c) and 5(d). In addition, the regularizing term attenuates the outer regions of the nebula, Figure 5(b). The stair-step artifacts are due to intensity discretization in the renderer.

For all axisymmetric reconstructions, the view along the axis of symmetry is only weakly constrained by the input image. It therefore depends mostly on the characteristics of the reconstruction algorithm and reveals typical artifacts that are not easily recognized in other projections. In our reconstruction of M2–9, artifacts appear in the form of radial banding due to the discrete radial groups, Figure 6(a). They are somewhat more obvious when displayed with a logarithmic intensity scale, Figure 6(b). In [WAG\*12], in contrast, artifacts are present in the form of streaks, Figure 6(c), which become even more obvious on a logarithmic scale, Figure 6(d), or when animated (see the accompanying video). These streaks are produced by the discretization of projection directions.

While our method avoids strong directional discretization artifacts in the form of streaks, radial banding could, in principle, be avoided by assigning each voxel to multiple adjacent groups with appropriate weighting factors. However,

**Table 1:** Reconstruction times for different data sets.

object	angle	volume size	runtime
Calabash	0°	240 × 440 × 240	42 s
HD 44179	0°	340 × 512 × 340	118 s
IC 418	0°	350 × 460 × 350	111 s
M2–9	0°	122 × 512 × 122	15 s
M2–9	0°	664 × 2824 × 664	3080 s
M57	0°	356 × 356 × 512	128 s
M57	90°	356 × 356 × 512	245 s
Mz 3	0°	235 × 512 × 235	51 s
Mz 3	30°	235 × 512 × 460	130 s
NGC 6302	0°	277 × 405 × 277	53 s
NGC 6826	0°	411 × 512 × 411	176 s
NGC 7009	0°	230 × 512 × 230	45 s

since this problem is not group separable, it requires a different and presumably more time-consuming algorithm. A possible solution would be to minimize the sum of two regularization terms

$$\arg \min_{\rho_1, \rho_2} \sum_i |G_i| \max \rho_1_{\{G_i\}} + \sum_i |H_i| \max \rho_2_{\{H_i\}} \quad (9)$$

subject to  $(P, \mathbb{I})^\top \rho_1 + (P, -\mathbb{I})^\top \rho_2 = (2s, 0)^\top$  with different group assignments  $G$  and  $H$ , each of which is separable. This could be achieved efficiently with an appropriate algorithm (e.g., [BPC\*11]). Alternatively, by using a particle-based approach [GKHH12], the discretization problem could be circumvented completely.

## 8 Conclusion

We have presented a novel algorithm for the reconstruction of approximately symmetric volumetric phenomena, like many astronomical nebulae, from single images. While we have demonstrated it on emissive phenomena, it can also be applied to absorbing objects by transforming the problem to a negative logarithmic scale; more complex linear image formation models can be substituted as well. The method generates plausible models for axisymmetric objects and can in principle be extended to objects with more complicated types of symmetry by specifying a custom symmetry model. It avoids typical artifacts present in prior work, such

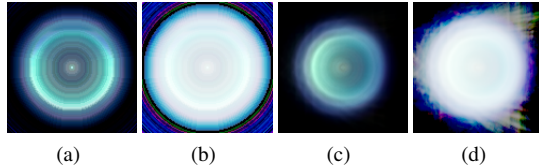


**Figure 6:** Artifacts visible in reconstructions of M2–9 when rendered from a viewpoint on the axis: our algorithm with linear (a) and logarithmic (b) color mapping, and [WAG\*12] with linear (c) and logarithmic (d) color mapping. Note the radial banding in our result, and the streaks in the prior work.

as streaks and unrealistic discontinuities during viewpoint changes.

Perhaps most importantly, our approach outperforms prior work by several orders of magnitude in terms of computation time, and is not limited by GPU memory. It thereby for the first time allows content creators to perform automatic reconstructions in high quality without any specialized hardware, expert knowledge or modeling experience.

## Acknowledgments

The present work was partially funded by Deutsche Forschungsgemeinschaft DFG project MA 2555/7–1 (“Astrographik”).

## References

- [BPC\*11] BOYD S., PARIKH N., CHU E., PELEATO B., ECKSTEIN J.: Distributed optimization and statistical learning via the alternating direction method of multipliers. *Foundations and Trends in Machine Learning* 3, 1 (2011), 1–122. [6](#)
- [BT09] BECK A., TEBOLLE M.: A fast iterative shrinkage-thresholding algorithm for linear inverse problems. *SIAM Journal on Imaging Sciences* 2, 1 (2009), 183–202. [4](#)
- [DSSC08] DUCHI J., SHALEV-SHWARTZ S., SINGER Y., CHANDRA T.: Efficient projections onto the  $\ell_1$ -ball for learning in high dimensions. In *Proceedings of the 25th International Conference on Machine Learning* (2008), pp. 272–279. [4](#)
- [FR08] FORNASIER M., RAUHUT H.: Recovery algorithms for vector-valued data with joint sparsity constraints. *SIAM J. Numerical Analysis* 46, 2 (2008), 577–613. [4](#)
- [GDLS\*11] GARCÍA-DÍAZ T., LÓPEZ J. A., STEFFEN W., RICHER M. G., RIESGO H.: A Cat’s Eye view of the Eskimo from Saturn. In *Proceedings of the IAU Symposium 283 “Planetary Nebulae: An Eye to the Future”* (2011), pp. 119–120. [2](#)
- [GKHH12] GREGSON J., KRIMERMAN M., HULLIN M. B., HEIDRICH W.: Stochastic tomography and its applications in 3D imaging of mixing fluids. *ACM Transactions on Graphics* 31, 4 (2012), 52:1–52:10. [6](#)
- [KS05] KWOK S., SU K.: Discovery of multiple coaxial rings in the quadrupolar planetary nebula NGC 6881. *The Astrophysical Journal Letters* 635, 1 (2005), L49–L52. [2](#)
- [Kwo07] KWOK S.: *The origin and evolution of planetary nebulae*, vol. 33. Cambridge University Press, 2007. [2](#)
- [Lea91] LEAHY D. A.: Deprojection of emission in axially symmetric transparent systems. *Astronomy and Astrophysics* 247 (1991), 584–589. [3](#)
- [MdFPL04] MÉKARNIA D., DE FREITAS PACHECO J. A., LAGADEC E.: 3D structure of the planetary nebula NGC 7027. In *Asymmetrical Planetary Nebulae III: Winds, Structure and the Thunderbird* (2004), Meixner M., Kastner J. H., Balick B., Soker N., (Eds.), vol. 313 of *Astronomical Society of the Pacific Conference Series*, pp. 119–122. [2](#)
- [MFG11] MONTEIRO H., FALCETA-GONÇALVES D.: Three-dimensional photoionization structure and distances of planetary nebulae. IV. NGC 40. *The Astrophysical Journal* 738 (2011), 174–183. [2](#)
- [MHLH05] MAGNOR M., HILDEBRAND K., LINTU A., HANSEN A.: Reflection nebula visualization. In *Proceedings of IEEE Visualization* (2005), pp. 255–262. [3](#)
- [MKHD04] MAGNOR M., KINDLMANN G., HANSEN C., DURIC N.: Constrained inverse volume rendering for planetary nebulae. In *Proceedings of IEEE Visualization* (2004), pp. 83–90. [3](#)
- [MKHD05] MAGNOR M., KINDLMANN G., HANSEN C., DURIC N.: Reconstruction and visualization of planetary nebulae. *IEEE Transactions on Visualization and Computer Graphics* 11, 5 (2005), 485–496. [3](#)
- [MSGH04] MONTEIRO H., SCHWARZ H. E., GRUENWALD R., HEATHCOTE S.: Three-dimensional photoionization structure and distances of planetary nebulae. I. NGC 6369. *The Astrophysical Journal* 609 (2004), 194–202. [2](#)
- [MW85] MEABURN J., WALSH J. R.: Echelle observations of high-velocity lobes projecting from the core of the bipolar nebula Mz 3. *Monthly Notices of the Royal Astronomical Society* 215 (1985), 761–771. [5](#)
- [NGN\*01] NADEAU D., GENETTI J., NAPEAR S., PAILTHORPE B., EMMART C., WESSELAK E., DAVIDSON D.: Visualizing stars and emission nebulas. *Computer Graphics Forum* 20, 1 (2001), 27–33. [2](#)
- [SKW\*11] STEFFEN W., KONING N., WENGER S., MORISSET C., MAGNOR M.: Shape: A 3D modeling tool for astrophysics. *IEEE Transactions on Visualization and Computer Graphics* 17, 4 (2011), 454–465. [2](#)
- [SM06] SCHWARZ H. E., MONTEIRO H.: Three-dimensional photoionization structure and distances of planetary nebulae. III. NGC 6781. *The Astrophysical Journal* 648 (2006), 430–434. [2](#)
- [STR\*06] SABBADIN F., TURATTO M., RAGAZZONI R., CAPPELLARO E., BENETTI S.: The structure of planetary nebulae: theory vs. practice. *Astronomy and Astrophysics* 451, 3 (2006), 937–949. [2](#)
- [WAFMM09] WENGER S., AJA FERNÁNDEZ J., MORISSET C., MAGNOR M.: Algebraic 3D reconstruction of planetary nebulae. *Journal of WSCG* 17, 1 (2009), 33–40. [3](#)
- [WAG\*12] WENGER S., AMENT M., GUTHÉ S., LORENZ D., TILLMANN A., WEISKOPF D., MAGNOR M.: Visualization of astronomical nebulae via distributed multi-GPU compressed sensing tomography. *IEEE Transactions on Visualization and Computer Graphics (TVCG, Proc. Visualization / InfoVis)* 18, 12 (2012), 2188–2197. [2, 3, 5, 6, 7](#)
- [WNF09] WRIGHT S. J., NOWAK R. D., FIGUEIREDO M. A. T.: Sparse reconstruction by separable approximation. *IEEE Transactions on Signal Processing* 57, 7 (2009), 2479–2493. [4](#)

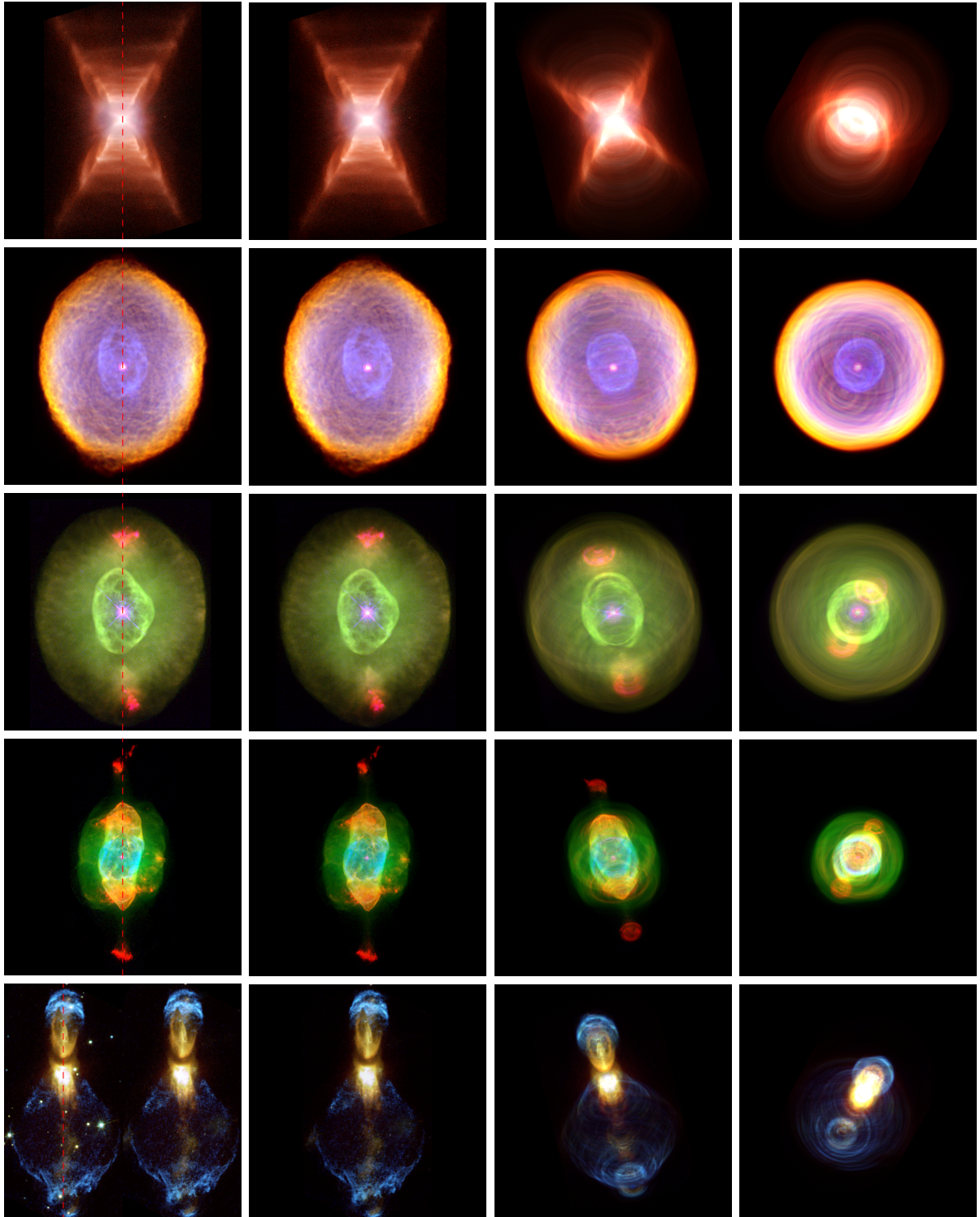


**Figure 7:** Additional reconstruction results. From left to right: original image, reconstruction rendered from original viewpoint, novel views. From top to bottom: HD 44179, IC 418, NGC 6826, NGC 7009, Calabash Nebula. Stars have been removed for the Calabash Nebula; original image and edited version are shown side by side. Original image credits: NASA/ESA and Hubble Space Telescope/The Hubble Heritage Team (STScI/AURA).